EAI Endorsed Transactions
on Sustainable Manufacturing and Renewable Energy Research Article EAI.EU

Optimizing Casting Processes with Rotating Magnetic Fields: Influence on Metal Solidification and Microstructure Homogeneity

Thanh Phat Tran[1], Hai Nguyen Diec[1], Thanh Phong Nguyen[1], Quoc Bao Lam[1], Quang Dat Nguyen[1] and Quang Thanh Le[2,*]

[1]University of Technology-VNU–HCM, Ho Chi Minh City, Vietnam
[2]Ho Chi Minh City University of Transport, Vietnam

Abstract

This study explores the effect of rotating magnetic fields on the quality of casting low-carbon steel. Magnetic casting influences the molten metal flow through a controlled permanent magnetic field, which optimizes heat dissipation and induces fluid stirring within the mold. Our simulations reveal that a rotating magnetic field can enhance crystal fragmentation and improve microstructure homogeneity by inducing a vortex in the superheated region of the molten metal. The impact of variables, including the distance and magnetic flux density of the permanent magnet, was analyzed, showing their influence on the molten metal flow and casting outcomes. Experimental results, supported by modeling, highlight that higher magnetic flux densities contribute to a more uniform microstructure. This approach can refine casting processes, reduce defects, and promote structural consistency. Our findings offer valuable insights for optimizing magnetic-assisted casting technologies for enhanced metal solidification and improved casting quality.

Keywords: Rotating Magnetic Fields, Magnetic Casting, Microstructure Homogeneity, Metal Solidification, Low-Carbon Steel Casting

Received on 08 11 2024, accepted on 16 11 2024, published on 17 01 2025

doi: 10.4108

1. Introduction

Steel is a crucial material used across various industries due to its versatility and strength, making it indispensable in manufacturing machinery, automotive components, and numerous other applications. The role of steel in modern life is pervasive, underscoring the need for continuous optimization of its production processes. This study specifically investigates the impact of magnetism generated by permanent magnets on the flow behavior of molten carbon steel during the casting process, with an emphasis on analyzing and evaluating its influence on casting outcomes.

Previous research has highlighted the potential of magnetic and electromagnetic stirring (M-EMS) methods to improve the solidification of molten metal. Studies like [1] demonstrated that M-EMS can enhance the flow of liquid metal and result in favorable solidification characteristics. During continuous casting, the solidification process can be manipulated through a magnetic field, although this is a complex phenomenon influenced by temperature, melting point, heat transfer, and mold conditions [2]. These factors not only affect heat transfer but also lead to stress and deformation in cast materials.

In attempts to optimize casting quality, [3] developed a comprehensive model using M-EMS for better control over liquid metal flow and heat transfer. Additionally, technologies like hot core rolling (HHR2) [4] have been employed, showing improvements in structural uniformity across the thickness of steel slabs. The proper implementation of M-EMS models, as analyzed through multiphysics simulations [5], reveals enhanced control over temperature and stress distribution in solidified steel shells. However, earlier studies tended to simplify the complex nature of

*Corresponding author. Email: Lequangthanh@ut.edu.vn

solidification by focusing solely on fibrous shell formation rather than equiaxed crystal development [6].
Numerical simulations employing multiphysics models have further illustrated that increasing M-EMS flow density results in changes in high-temperature regions and intensified subsurface separation [7]. Other comprehensive models [8] investigated M-EMS's impact on fluid flow, temperature gradients, solute concentration, and solidification behavior within cast blanks, indicating nearly uniform concentration distribution within the affected regions while leaving certain challenges, such as centerline segregation, unresolved.
Microstructure refinement through methods like electroslag refining (ESR) [9-12] has proven effective at eliminating non-metallic impurities, enhancing the homogeneity of the cast structure. Additional techniques for molten metal and slag reactions in electroslag casting [13] and particle separation control through M-EMS [14-15] have further advanced casting technology. While temperature-controlled melting is excluded from this study, comparable research by [16] indicates that high-temperature control remains relevant for optimizing casting outcomes.
This study aims to build upon these advancements by exploring the influence of rotating magnetic fields on molten metal flow and casting microstructure. Key areas of focus include optimizing magnetic flux density, evaluating its effect on microstructure homogeneity, and refining the casting process parameters. The findings presented herein offer new insights for enhancing casting quality and serve as a foundation for further innovations in magnetic-assisted casting technologies.

2. Experimental procedures

The illustration in Figure 1 depicts the schematic principle of a casting system utilizing a rotating magnetic field to influence the flow of molten metal during the casting process. The system comprises three stacked permanent magnets that generate a strong rotating magnetic field when placed near the mold. This magnetic field directly impacts the flow of molten metal within the mold, enhancing crystallization and microstructure uniformity. Beneath the magnets is a swivel tray that provides rotational motion, facilitating strong interaction between the magnetic field and the molten metal flow. The thin shell mold, positioned centrally within the system, holds the molten metal and shapes the cast product. As molten metal is poured into the mold, the rotating magnetic field induces changes in the microstructure, promoting crystallization and improving surface quality. The system demonstrates the optimization of casting processes by controlling magnetic field intensity and rotational dynamics to improve the final product's quality.

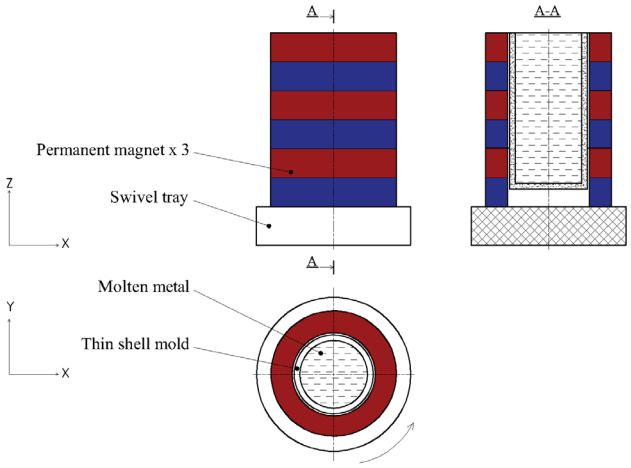

Figure 1. Magnetic casting diagram

Figure 2 depicts the magnetic field distribution around a cylindrical assembly of stacked permanent magnets with alternating North (N) and South (S) poles. The magnetic field lines emanate outward from the North poles and loop around to the South poles, creating a closed-loop pattern of flux lines surrounding the structure. This configuration demonstrates the concentrated and directional nature of the magnetic field generated by the stacked magnets. The arrows on the field lines indicate the direction of the magnetic flux, illustrating the behavior and flow of the magnetic field around the cylindrical magnets. Such a distribution is critical for applications involving magnetic field control, including its influence on molten metal flow during casting processes. This arrangement provides a strong and stable magnetic field capable of affecting the structure and flow dynamics of molten metals within a casting mold.

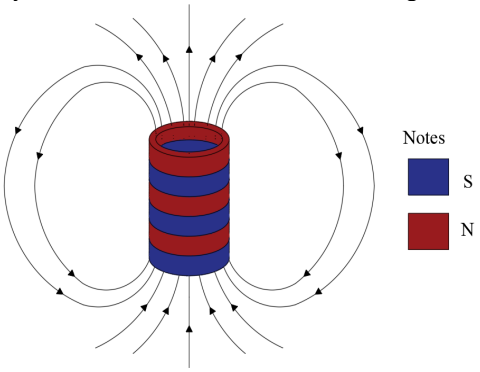

Figure 2. Magnetic Field Distribution Around Stacked Permanent Magnets

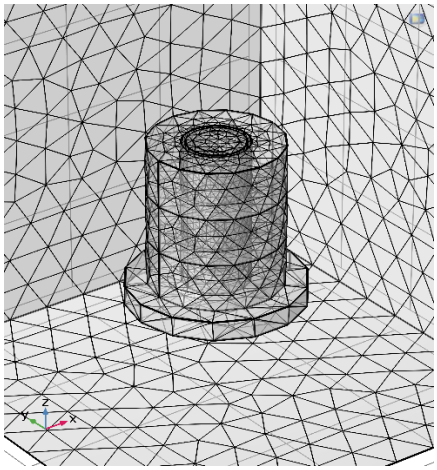

Figure 3. Meshed Model of a Cylindrical Permanent Magnet Assembly in a Computational Domain

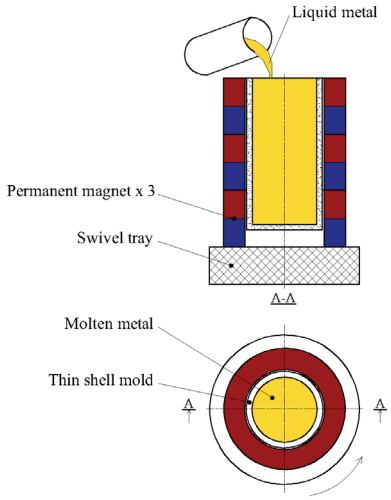

Figure 4. Schematic of Molten Metal Pouring into a Thin Shell Mold with Magnetic Field Influence

Figure 4 illustrates a schematic of molten metal being poured into a thin shell mold under the influence of a magnetic field generated by three stacked permanent magnets. The molten metal is poured vertically from above into the mold, which is surrounded by the cylindrical arrangement of magnets. These magnets create a rotating magnetic field intended to control and optimize the flow and solidification of the molten metal. The swivel tray beneath the magnet assembly facilitates rotational dynamics, enhancing the magnetic interaction with the metal flow. The cross-sectional view (A-A) and the top view of the system highlight the alignment of the mold and magnets, demonstrating how the magnetic field encapsulates and interacts with the molten metal. This setup is designed to improve casting quality by influencing microstructure formation and enhancing uniformity during the solidification process.

Low-carbon steel was utilized as the billet material in this study, with its chemical composition detailed in Table 1.

Figure 3 displays a meshed computational model of a cylindrical permanent magnet assembly within a defined simulation domain. The mesh structure consists of interconnected triangular elements that provide a high-resolution representation of the geometry, enabling detailed numerical simulations. The central cylindrical component, representing stacked permanent magnets, is surrounded by a dense mesh to ensure precise calculations of magnetic field behavior and its interaction with surrounding environments. This meshed configuration allows for accurate simulation of physical phenomena such as magnetic flux distribution, heat transfer, and interactions with molten metal flow. The computational domain depicted is crucial for performing finite element analysis (FEA) and other multiphysics simulations, supporting the study and optimization of magnetic casting processes and related technologies.

Table 1. Chemical composition for Low carbon steel 1018 (wt.%)

C	Si	Mn	P	S
0.14 - 0.2	0.6 – 0.9	1.65	0.04	0.05

The selection of material is crucial to ensure that the magnetic field effectively interacts with it. Additionally, the magnetic density plays a significant role in providing a sufficient impact on the mold. In this model, the magnet is designed with specific dimensions, as detailed in Table 2.

Table 2. N40(ndfeb) self-designed permanent magnet (wt.T)

Recoil permeability	Remanent flux density norm	Height (mm)
1.05	1.28	25

The experiment was carried out using parameters such as the inner diameter, the thickness of the inner and outer diameters, along with other fixed parameters listed in Table 3. A total of 15 simulated samples were conducted.

Table 3. Casting parameters levels

Inner diameter(mm)	26	28	30	32	34
Inner and outer diameter thickness(mm)	10	13	15	-	-
Rotary wheel speed(rpm)	60	60	60	60	60

The simulation data, including detailed survey points collected during the process, are presented in Table 4. Key data points include the inner diameter and thickness of the magnet. In comparison to other studies, this model is on a smaller scale, resulting in a magnetic field generated by the magnet that is also comparatively weaker.

Table 4. Central composite rotatable design matrix

N	Inner diameter (mm)	Inner and outer diameter thickness (mm)	Rotary wheel speed (rpm)
1	26	10	60
2	28	10	60
3	30	10	60
4	32	10	60
5	34	10	60
6	26	13	60
7	28	13	60
8	30	13	60
9	32	13	60
10	34	13	60
11	26	15	60
12	28	15	60
13	30	15	60
14	32	15	60
15	34	15	60

Several setup steps were performed in Comsol 5.6 software for the simulation. Upon completing the calculations, the results of the magnetic flux density norm are displayed in Figure 5.
Figure 5 presents the results of a simulation showing the magnetic flux density norm around a cylindrical magnet assembly, displayed as a multislice view within a 3D computational domain. The color gradient represents the strength of the magnetic flux density, with values ranging from a minimum of $6.15x10^{-5}$ T (indicated in dark blue) to a maximum of 1.18 T (shown in light colors). The magnetic field distribution is visualized across various cross-sections, highlighting the spatial variation of magnetic flux. The contours illustrate how the magnetic field propagates through the domain, interacting strongly near the magnet assembly and gradually decreasing further away. This visualization helps to analyze the effectiveness of the magnetic field in impacting processes such as molten metal flow during casting simulations.

Figure 6 illustrates the magnetic field distribution around a cylindrical magnet assembly in two cross-sections. Figure 6(a) (left) shows the YZ cross-section, where contour lines represent the intensity of the magnetic flux, with a dense concentration around the ends of the permanent magnets, indicating strong magnetic influence. This symmetrical pattern highlights the interaction and powerful effect of the magnetic field on surrounding regions, crucial for controlling molten metal flow during casting. Figure 6(b) (right) depicts the XY cross-section, with concentric contour lines emanating from the center, illustrating a radial distribution of magnetic flux intensity. The magnetic field is strongest near the magnet's core and gradually decreases outward, creating a uniform and controlled influence around the central axis, which is essential for shaping and optimizing molten metal behavior within the mold.

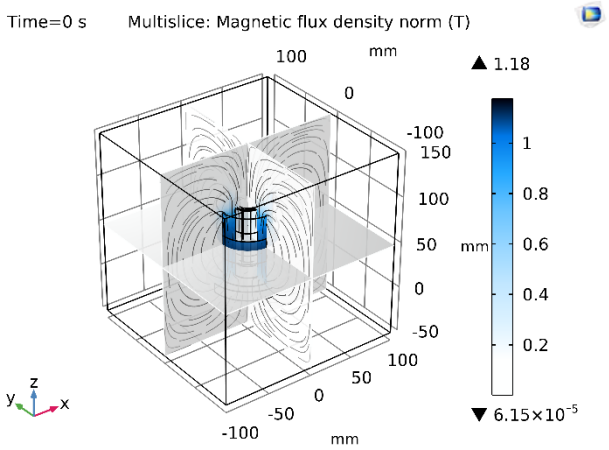

Figure 5. Simulation Result of Magnetic Flux Density Norm in Multislice View

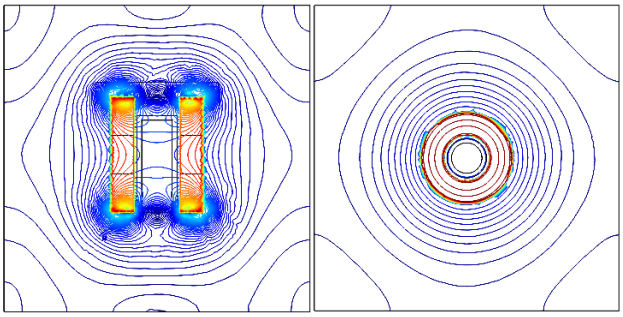

Figure 6. Magnetic Field Distribution in XY Cross-Section

3. Results and Discussion

Figure 7 illustrates three views of the survey points within the simulated domain of the cylindrical magnet assembly, each represented by a red point. Figure 7(a) (left) shows a frontal view, highlighting the position of the survey point in relation to the vertical axis of the magnet assembly, capturing its height and alignment within the domain. Figure 7(b) (middle) presents a side view, providing insight into the horizontal placement and relative positioning of the survey point along the magnetic axis. Figure 7(c) (right) depicts a top-down view, offering a perspective on the central alignment of the survey point with respect to the rotating assembly. Together, these figures illustrate the precise locations used to assess the magnetic field's impact within the simulation, ensuring a comprehensive understanding of the spatial distribution and influence of magnetic flux on the casting process.

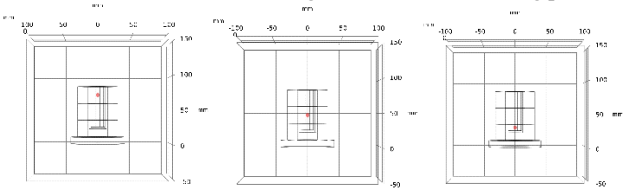

Figure 7. Survey Point Positions in the Simulated Domain of the Magnetic Field

Figure 8 displays a contour plot of the magnetic flux density norm around a cylindrical magnet assembly at 1 second. The plot illustrates the magnetic field distribution, with contour lines and a color gradient representing varying intensities of the flux density in Tesla (T). High-intensity regions are shown in red and yellow, indicating stronger magnetic fields around the ends of the magnets, while lower intensity areas are represented in blue. This distribution highlights the concentrated magnetic influence near the poles and the surrounding regions, demonstrating the field's interaction with the environment. The symmetric pattern of the field lines reveals the impact of the rotating magnetic field generated by the stacked permanent magnets, providing key insights into the field's behavior and its effect on processes such as molten metal flow during casting. The color bar on the right details the range of magnetic flux densities present in the simulation.

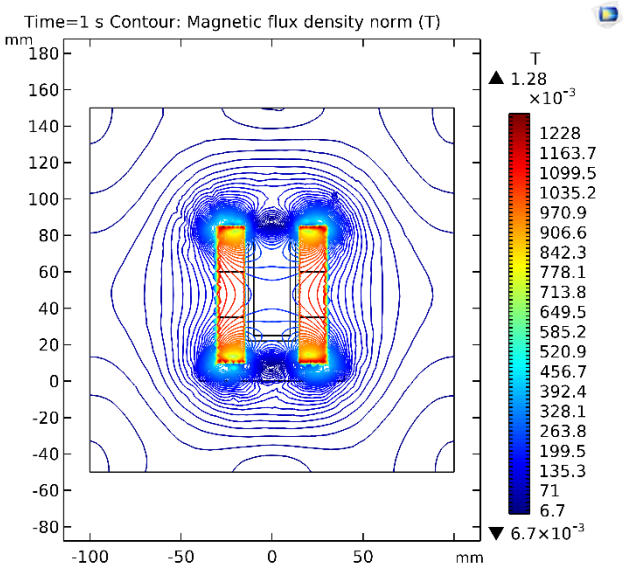

Figure 8. Contour Plot of Magnetic Flux Density Norm at 1 Second

Table 5 presents the Z-axis coordinates of three survey points used in the simulation study. These points are designated to capture magnetic field characteristics and their influence at different heights relative to the cylindrical magnet assembly. The Z-axis coordinates for each point are provided in millimeters (mm), with Point 1 located at 72.5 mm, Point 2 at 47.5 mm, and Point 3 at 30 mm. This arrangement allows for an in-depth analysis of magnetic field variations and their impact across different sections of the simulated domain, supporting the evaluation of field strength and distribution in relation to the casting process.

Table 5. Survey Point Coordinates along the Z-Axis

Point	Z axis coordinates (mm)
1	72.5
2	47.5
3	30

Table 6 lists the magnetic flux density values, measured in Tesla (T), at three designated survey points within the simulated domain. Each row corresponds to a unique simulation case (N) and displays the magnetic flux density values at Point 1, Point 2, and Point 3, reflecting their respective Z-axis coordinates as defined earlier. These values illustrate variations in the magnetic field strength at different locations within the domain, providing critical insights into how the magnetic flux interacts across the height of the cylindrical magnet assembly. The data enables the assessment of field intensity distribution, offering valuable information for optimizing magnetic influence in processes like molten metal flow during casting simulations.

Table 6. Values at points

N	Point 1 (T)	Point 2 (T)	Point 3 (T)
1	0.17117	0.12811	0.15816
2	0.16855	0.13091	0.15773
3	0.16267	0.13434	0.15758
4	0.15594	0.13649	0.1564
5	0.14875	0.13897	0.15542
6	0.21222	0.17045	0.20317
7	0.20411	0.17327	0.20259
8	0.19899	0.1775	0.20128
9	0.19525	0.18031	0.2001
10	0.18846	0.18231	0.19842
11	0.23735	0.19944	0.23233
12	0.23059	0.20296	0.23098
13	0.22314	0.20545	0.22963
14	0.21938	0.20907	0.22819
15	0.21058	0.2117	0.22596

Figure 9 illustrates the magnetic field lines and flow distribution around the cylindrical magnet assembly in two cross-sections. Figure 9(a) (left) shows the YZ cross-section, highlighting the magnetic lines of flux around the vertical assembly. Red dashed lines represent the magnetic field's direction, demonstrating concentrated magnetic influence around the magnets and symmetric flux patterns extending outward. Figure 9(b) (right) depicts the XY cross-section, with concentric magnetic lines radiating from the central axis of the magnets. The red arrows indicate the direction of the field, showcasing a radial distribution of flux around the cylindrical structure. Together, these figures emphasize the uniform and strong magnetic field distribution generated by the stacked magnets, crucial for applications such as controlling molten metal flow in casting processes.

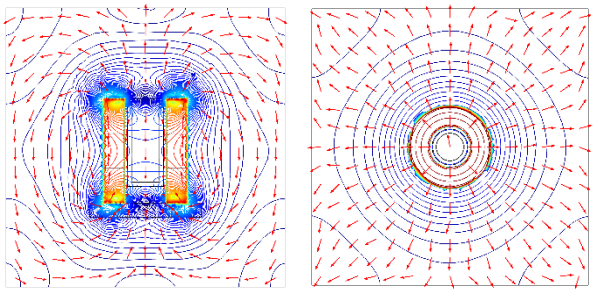

Figure 9. Magnetic Field Lines and Flux Distribution in YZ and XY Cross-Sections

Table 7 presents the central composite design matrix used to evaluate the impact of different casting parameters on the magnetic field influence (Δz) in Tesla (T). The table lists 15 experiments (N), each defined by three key variables: inner diameter (mm), inner and outer diameter thickness (mm), and rotary wheel speed (rpm), all maintained at a constant value of 60 rpm. The resulting Δz values represent the magnetic field's influence, varying according to changes in the inner diameter and thickness of the magnet assembly. This matrix allows for an in-depth analysis of the relationship between casting parameters and the magnetic field effect, facilitating optimization of magnetic casting processes.

Table 7. Central Composite Design Matrix of Casting Parameters and Magnetic Field Impact (Δz)

N	Inner diameter (mm)	Inner and outer diameter thickness (mm)	Rotary wheel speed (rpm)	Δz (T)
1	26	10	60	0.15248
2	28	10	60	0.1524
3	30	10	60	0.15153
4	32	10	60	0.14961
5	34	10	60	0.14771
6	26	13	60	0.19528
7	28	13	60	0.19332
8	30	13	60	0.19259
9	32	13	60	0.19189
10	34	13	60	0.18973
11	26	15	60	0.22304
12	28	15	60	0.22151
13	30	15	60	0.21941
14	32	15	60	0.21888
15	34	15	60	0.21608

Table 8 presents the coded coefficients of the regression model used to evaluate the influence of different casting parameters on the magnetic field's effect in the system. The terms listed include the constant, parameter $x_2.x_2$ (inner and outer diameter thickness), parameter $x_3.x_3$ (survey point along the Z-axis), and their interaction term $x_3*x_3.x_3*x_3$. The coefficients (Coef), standard errors (SE Coef), T-values, P-values, and Variance Inflation Factors (VIF) are provided for each term. The high significance of $x_2.x_2$ and $x_3.x_3$ is indicated by their low P-values (0.000), suggesting a strong impact on the model. The VIF values highlight multicollinearity among the parameters, especially for $x_3.x_3$ and $x_3*x_3.x_3*x_3$. This table supports the statistical analysis of factor influences and interactions, contributing to the optimization of magnetic casting processes.

Table 8. Coded Coefficients of Regression Model for Magnetic Casting Parameters

Term	Coef	SE Ceof	T-Value	P-Value	VIF
Constant	0.1187	0.0226	5.26	0.001	
x_2	0.013792	0.000872	15.81	0.000	1
x_3	-0.004793	0.00079	-6.07	0.000	68.38
x_3*x_3	0.000047	0.000007	6.44	0.000	68.38

Table 9 presents the Analysis of Variance (ANOVA) for studying the influence of magnetic casting parameters. The table includes the source of variation (Model, Linear terms, Square terms, and Error), degrees of freedom (DF), adjusted sums of squares (Adj SS), adjusted mean squares (Adj MS), F-values, and P-values. The high F-values and low P-values for terms $x_2.x_2$ (inner and outer diameter thickness) and $x_3.x_3$ (survey point along the Z-axis) indicate their significant impact on the model. The linear and interaction terms, such as $x_3*x_3.$ x_3* x_3, also exhibit a notable influence, reflected by their statistical significance. The ANOVA analysis helps determine the contributions of each factor and interaction, validating the regression model's accuracy in predicting the effect of magnetic fields in the casting process.

Table 9. Analysis of Variance (ANOVA) for the Regression Model of Magnetic Casting Parameters

Source	DF	Adj SS	Adj MS	F-Value	P-Value
Model	3	0.011840	0.003947	102.31	0.000
Linear	2	0.011342	0.005671	147.01	0.000
x_2	1	0.009644	0.009644	250.01	0.000
x_3	1	0.001419	0.001419	36.8	0.000
Square	1	0.001598	0.001598	41.44	0.000
x_3*x_3	1	0.001598	0.001598	41.44	0.000
Error	9	0.000347	0.000039		
Total	12	0.012187			

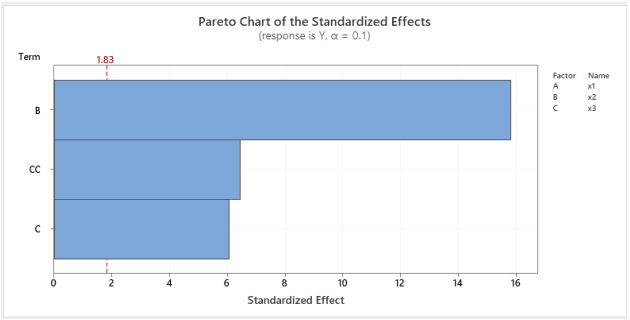

Figure 10. Pareto Chart of the Standardized Effects for Magnetic Casting Parameters

Figure 10 displays a Pareto chart illustrating the standardized effects of different parameters on the response variable in the magnetic casting process. The chart ranks the magnitude and significance of factors and their interactions, represented by bars in descending order of standardized effect size. The vertical red line indicates the threshold of statistical significance. Factors labeled as *B* (inner and outer diameter thickness) and their interaction terms surpass this threshold, demonstrating their substantial impact on the response. Parameters with bars extending beyond this line are considered statistically significant, indicating that these factors critically influence the model's behavior and output. This visualization helps identify the most influential factors, aiding in the optimization of the casting process by focusing on the parameters that exert the greatest

control over the magnetic field's impact on molten metal flow and solidification.

The analysis of the Design of Experiments (DOE) and experimental data provides valuable insights into the influence of various factors and their interactions on the response variables. As shown in Tables 8 and 9, the study evaluates how the survey location affects the inner and outer diameter thickness ($x_2x_2x_2$) as well as the survey point along the Z-axis ($x_3x_3x_3$). The low P-values (0) and high F-values (250.01 and 36.80, respectively) suggest that changes in either the inner and outer diameter thickness or the Z-axis survey location significantly impact casting quality and performance. Increasing these factors can have positive or negative effects on the casting process, as indicated by their statistical significance. During the analysis, any non-significant survey intervals with P-values greater than 0.5 were excluded.

The regression equation derived from the data analysis is as follows:

$$Y = 0.1187 + 0.013792\ x_2 - 0.004793\ x_3 + 0.000047\ x_3 * x_3$$

This equation represents the influence of the independent variables and their interactions, computed using the DOE methodology, allowing for accurate predictions and insights into the casting process's behavior.

Table 10. Regression Model Performance Metrics

S	R-sq	R-sq (adj)	R-sq (pred)
0.0062109	97.15%	96.20%	94.43%

Table 10 summarizes the performance metrics of the regression model used in the analysis. The values include the standard error of the regression (S = 0.0062109), the coefficient of determination (R-sq = 97.15%), the adjusted R-squared (R-sq adj = 96.20%), and the predicted R-squared (R-sq pred = 94.43%). These high R-squared values indicate a strong fit between the model and the data, demonstrating that the model effectively explains the variability in the response variables and provides reliable predictions.

Figure 11 shows the normal plot of the standardized effects for the response variable YY. The plot indicates which factors and interactions are significant by displaying their standardized effects relative to a reference line. Points that deviate notably from the line, such as factors labeled BB (inner and outer diameter thickness) and CC (survey point along the Z-axis), are considered significant. This plot helps to visually assess the impact of different parameters on the response and identify those with the most substantial influence.

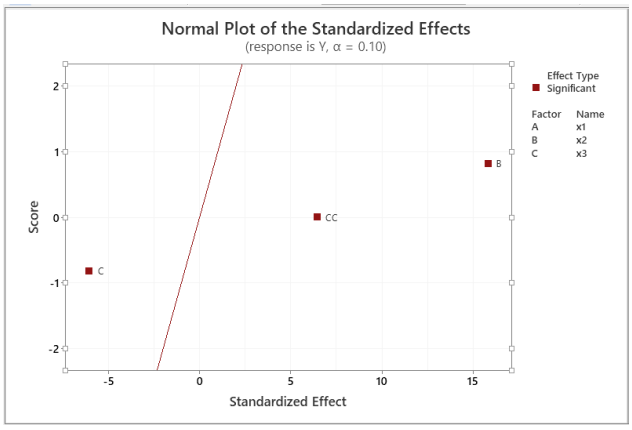

Figure 11. Normal Plot of the Standardized Effects

4. Conclusion

This study examined the influence of rotating magnetic fields on the casting process of low-carbon steel, focusing on optimizing microstructure homogeneity. Key findings include a significant impact of inner and outer diameter thickness ($x_2.x_2$) and Z-axis survey location ($x_3.x_3$) on casting quality, as evidenced by low P-values (0) and high F-values (250.01 and 36.80, respectively). The regression model demonstrated a strong fit with an R-squared value of 97.15%, indicating robust predictive capability. Simulation results highlighted variations in magnetic flux density, with values reaching up to 1.28 T in concentrated regions, providing critical insights into field distribution. This work offers valuable guidance for improving casting quality through precise magnetic field control and parameter optimization.

Acknowledgements.

We acknowledge the support of time and facilities from Ho Chi Minh City University of Technology (HCMUT), VNU-HCM for this study

References

[1] Zhang, Z., et al., Modeling of the as-cast structure and macrosegregation in the continuous casting of a steel billet: Effect of M-EMS. Journal of materials processing technology, 2022. 301: p. 117434.

[2] Du, F., et al., Investigation on non-uniform friction behaviors of slab during continuous casting based on an inverse algorithm. Journal of Materials Processing Technology, 2021. 288: p. 116871.

[3] Thomas, B.G., Review on modeling and simulation of continuous casting. steel research international, 2018. 89(1): p. 1700312.

[4] Li, H., et al., Effects of hot-core heavy reduction rolling during continuous casting on microstructures and mechanical properties of hot-rolled plates. Journal of Materials Processing Technology, 2020. 283: p. 116708.

[5] Zappulla, M.L., et al., Multiphysics modeling of continuous casting of stainless steel. Journal of Materials Processing Technology, 2020. 278: p. 116469.

[6] Zhang, W., et al., Numerical simulation of fluid flow, heat transfer, species transfer, and solidification in billet continuous casting mold with M-EMS. Metals, 2019. 9(1): p. 66.
[7] Trindade, L.B., J.E.A. Nadalon, A.C. Contini, and R.C. Barroso, Modeling of solidification in continuous casting round billet with mold electromagnetic stirring (M-EMS). steel research international, 2017. 88(4): p. 1600319.
[8] Fang, Q., et al., Effects of EMS induced flow on solidification and solute transport in bloom mold. Metals, 2017. 7(3): p. 72.
[9] Sharpe, R., G. Benfield, G. Roberts, and R. Francis, The undergraduate experience of blended e-learning: a review of UK literature and practice. The higher education academy, 2006. 4(2): p. 24-250.
[10] Xinxu, L., et al., Segregation and homogenization for a new nickel-based superalloy. Vacuum, 2020. 177: p. 109379.
[11] Podgornik, B., V. Leskovšek, M. Godec, and B. Senčič, Microstructure refinement and its effect on properties of spring steel. Materials Science and Engineering: A, 2014. 599: p. 81-86.
[12] Sabih, A., P. Wanjara, and J. Nemes, Characterization of internal voids and cracks in cold heading of dual phase steel. ISIJ international, 2005. 45(8): p. 1179-1186.
[13] Zhong, Y.-b., et al., Effect of transverse static magnetic field on microstructure and properties of GCr15 bearing steel in electroslag continuous casting process. Materials Science and Engineering: A, 2016. 660: p. 118-126.
[14] Wang, S., G.A. De Toledo, K. Välimaa, and S. Louhenkilpi, Magnetohydrodynamic phenomena, fluid control and computational modeling in the continuous casting of billet and bloom. ISIJ International, 2014. 54(10): p. 2273-2282.
[15] Li, S., et al., Analysis on electromagnetic field of continuous casting mold including a new integral method for calculating electromagnetic torque. Metals, 2019. 9(9): p. 946.
[16] Han, Q. and A. Hellawell, Primary particle melting rates and equiaxed grain nucleation. Metallurgical and Materials Transactions B, 1997. 28(1): p. 169-173.